April 7th 2022

Rivers of the Variscan Foreland: fluvial morphodynamics in the Pennant Formation of South Wales, UK

James Wood[1*], Jonah S. McLeod[1], Sinéad J. Lyster[1] and Alexander C. Whittaker[1]

[1]Department of Earth Science and Engineering, Imperial College London, UK, SW7 2BX.

*Correspondence (james.wood18@imperial.ac.uk)

note the above email will expire after July 2022 – alternatives include: a.whittaker@imperial.ac.uk, s.lyster17@imperial.ac.uk & jonah.mcleod18@imperial.ac.uk

Present address: (AW) 3.51, Royal School of Mines, South Kensington Campus, Prince Consort Road, London SW7 2AZ

Abbreviated title: Rivers of the Variscan Foreland

ORCiDs: JW – 0000-0002-1673-0097, JM – 0000-0002-5382-3559, SL - 0000-0002-1188-533X, AW - 0000-0002-8781-7771.

Abstract

The morphodynamics of ancient rivers can be reconstructed from fluvial stratigraphy using quantitative techniques to provide detailed insights into the driving forces behind the sedimentary systems. This work explores how these drivers can be evaluated from Paleozoic stratigraphy. Field measurements are taken in fluvial sediments from the Westphalian (Bolsovian and Asturian; 315.2–308 Ma) Pennant Formation of South Wales, UK, to reconstruct the hydrodynamics and morphologies of these Carboniferous rivers, which were sourced from the Variscan (Hercynian) Mountain belt located south of the study area. Field data consist of cross-set heights, grain size, palaeocurrent directions, and the dimensions of fluvial architectural elements. Hydrodynamic properties, including flow velocities and discharge rates, are reconstructed using a suite of numerical approaches. Results suggest median formative flow depths of 2–3 m and palaeoslopes of 4-5 × 10^{-4} (0.02–0.03°). Quantitative planform prediction suggests these rivers were likely anastomosing but with distinct single-threaded reaches. Mean single-thread width is 55 m, while mean channel-belt widths of 100–200 m are reconstructed, suggesting bankfull discharges of 390–560 $m^3 s^{-1}$. This study resolves contrasting palaeohydrological interpretations for Pennant rivers, and demonstrates how sophisticated reconstructions of morphology, slope and planform can be obtained from fluvial stratigraphy.

Supplementary Material

Field data, a field localities KMZ file, analysis of flow depth scaling methods, and fluvial facies analysis is available at xxxxxxxx.

Rivers have been among the most significant drivers of geomorphological and hydrological change on Earth's surface since the Precambrian (Hjellbakk 1997; Eriksson et al. 2006; Gibling & Davies 2012; Ielpi et al. 2017; Ganti et al. 2019). Their hydrodynamic and morphodynamic properties are recorded in the stratigraphic record (Whittaker 2012; Ganti et al. 2014, Bhattacharya et al. 2016), allowing researchers to reconstruct the characteristics and behaviour of ancient fluvial systems from the geological archive (e.g., Michael et al. 2014; Ganti et al. 2019; Chamberlin & Hajek 2019; Lyster et al. 2021). These reconstructions include morphologic and hydrodynamic properties (Paola & Mohrig 1996; Duller et al. 2012; Chen et al. 2018; Shibata et al. 2018; Greenberg & Hajek 2021), sediment transport capacity (Holbrook and Wanas 2014; Li & Bhattacharya 2017; Sharma et al. 2017; Mahon and McElroy 2018), and drainage area and shape (Bhattacharya and Tye 2004; Bhattacharya et al. 2016; Xu et al. 2017; Li et al. 2018; Lyster et al., 2020). As river development is closely linked to tectonic and climatic forcing, fluvial strata provide insights into the prevailing tectono-climatic conditions at the time of deposition (Duller et al. 2010; Castelltort et al. 2012; Whittaker 2012; Harries et al. 2021).

While much work in the field of sedimentology has typically implemented qualitative techniques (e.g., facies analysis) to decipher river characteristics from fluvial strata (e.g., Jones 1977; Miall 1985; Bridge 2003; Plink-Bjorklund 2015, amongst many others), an increasing number of quantitative investigations are beginning to present new opportunities within the discipline. Empirical equations are often used to describe the morphology and hydrology of modern rivers in terms of slope, depth, and water discharge (Leopold and Maddock Jr. 1953; Hack 1957; Leopold and Wolman 1960; Williams 1984). These methods have been adapted for stratigraphic application to facilitate multifaceted reconstructions of ancient systems (Bridge and Mackey 1992; Leclair and Bridge 2001; Trampush et al. 2014; Bradley and Venditti 2017; Greenberg et al. 2021), enabling fluvial morphodynamics to be quantified in a way that is not possible from qualitative facies analyses alone. However, quantitative palaeohydrological techniques can be restricted by the incomplete nature of the rock record (Sadler 1981; Straub et al. 2020) and the limited data sets to-date of ancient river deposits where important sedimentological observables, such as height and distributions of cross-beds, are quantified with sufficient precision to enable robust reconstructions (c.f. Leary & Ganti 2019; Lyster et al. 2022).

Nonetheless, in principle, palaeohydrological studies offer a unique opportunity to reconstruct ancient fluvial landscapes, particularly where the corresponding geomorphic archive has been lost, and to quantify the fluxes of sediment and water across the surface of the Earth and other planets in the geological past (Ganti et al. 2019; Stack et al. 2019; Lyster et al. 2021).

This study focuses on the palaeohydrology of Upper Carboniferous (Pennsylvanian) fluvial systems of the Pennant Sandstone Formation, South Wales, UK (Figure 1). In the UK, the Upper Carboniferous comprises the Namurian, Westphalian, Stephanian and Autunian regional stages, with the Westphalian stage, which is the subject of this study, spanning 315.2 Ma to 307 Ma. Further, the Westphalian stage comprises the Langsettian, Duckmantian, Bolsovian and Asturian regional substages, with the Bolsovian and Asturian substages being the focus here (315.2−308 Ma).

The Pennant Sandstone is of key interest due to its tectono-geographic setting in the foreland of the Variscan Orogen, temporally close to the cessation of the northward migration of the Variscan front during the Westphalian stage (Gayer and Jones 1989; Jones 1991; Burgess and Gayer 2000; Opluštil and Cleal 2007). Hence, these strata record the behaviour, water discharges, and sediment fluxes of rivers during the latter stages of the assembly of the Pangaean supercontinent. The formation crops out extensively in the South Wales and Pembrokeshire Coalfields and has a well-constrained stratigraphic framework owing to geological studies during Wales' time as a productive coal mining region (Woodland et al. 1957; Kelling 1974; Jones 1977). Previous sedimentological work on the Pennant has largely centred on facies and architectural observations, the majority of which were qualitative in nature (De la Beche 1846, Strahan 1899, Woodland et al. 1957, Kelling 1974, Jones 1977; Jones & Hartley, 1993). To date, the morphodynamic and hydrodynamic characteristics of these fluvial systems have not been reconstructed using quantitative techniques, meaning that our understanding of their behaviour, their relationship with the Variscan Front, and ultimately their evolution, is incomplete. Here we revisit the Pennant Formation and use quantitative palaeohydrological approaches, founded in bedform analysis (c.f. Ganti et al. 2019; Lyster et al. 2021), to exemplify how new insights into fluvial system behaviour can be obtained for "classic" geological formations that have received little recent study. Consequently, our field data from the Pennant Formation allow us to reconstruct flow depths, palaeoslopes, water discharges, and planform morphologies for Pennant palaeo-rivers at multiple spatio-temporal intervals.

Regional Tectono-stratigraphy

The Pennant Sandstone Formation comprises Bolsovian and Asturian aged fluvial sediments that were deposited in the South Wales foreland basin (Figure 1a) by rivers draining mountainous terrain built during the Variscan orogeny which, at the time, was located to the south of the study area (Kelling

1974; Evans 2004). Today, these sediments crop out in the South Wales and Pembrokeshire Coalfields. The Variscan (Hercynian) Orogeny was the principal formative orogenic event of the supercontinent Pangaea, creating an orogenic belt that stretched east–west over 1000 km (Leveridge and Hartley 2006). Many of the north–south orientated compressional structures and sedimentary basins of Europe today can be attributed to the Variscan Orogeny, including the South Wales and Pembrokeshire coalfields that form the geographical focus of this study (Leveridge and Hartley 2006, Opluštil and Cleal 2007). The South Wales foreland basin, situated to the north of the northward propagating Variscan Orogenic Belt (Figure 1c), was generated following inversion of a regional Devonian–Lower Carboniferous extensional regime (Hartley and Warr 1990; Burgess and Gayer 2000; Opluštil and Cleal 2007). The northern edge of the foreland was bounded by the cratonic upland of the Wales-Brabant High (Figure 1c; Rippon 1996).

By the end of the Carboniferous, the front of Variscan deformation had migrated northward to the location of the South Wales Coalfield, producing shortening of up to 30% and north–south compressional structures such as the major asymmetric syncline that dominates the structure of the coalfield today (Figure 1b; Jones 1991; Gayer and Pesek 1992; Evans 2004). Subsidence curves of the South Wales Basin suggest a rapid accommodation generation of 260 m Myr^{-1} in the west and 130 m Myr^{-1} in the east during the late Westphalian (Burgess and Gayer 2000). As the underlying South Wales Coal Measures consist of sediment sourced from the Wales-Brabant High (Evans 2004), the base of the Pennant Formation represents the onset of Variscan deposition in the region (Leveridge and Hartley 2006; Opluštil and Cleal 2007).

The Pennant sandstone has a maximum total thickness of 1350 m and is subdivided into 5 members shown in Figure 2 (Barclay 2011). These members, first described as 'beds' by Woodland et al. (1957) following the early classification work of De La Beche (1846) and Strahan (1899), are separated by coal horizons and form the basis for temporal differentiation in this study. Each member contains sandstone (greenish-grey, lithic arenite), mudstone, siltstone, and coals of varying abundances and thicknesses (Waters et al. 2007; Waters et al. 2009). The Rhondda Member is the thickest and contains the highest proportion of sand (Waters et al. 2009) so is, therefore, the most represented member in outcrop. The Llynfi, Hughes, and Swansea members have limited outcrop due to higher proportion of muds and silts, while the Brithdir Member's lesser thickness also limits the abundance of outcrop (Waters et al. 2009). While the exact stratigraphic boundary between the Bolsovian and Asturian substages is not formally defined in the Pennant Sandstone, it is considered to be within the Brithdir Member's depositional timespan (Waters et al. 2009; Barclay 2011).

The base of the Pennant Formation is described as the first significant ‘Pennant-type’ sandstone (greenish-grey and blueish-grey, feldspathic, micaceous, lithic arenite) of at least 3 m thickness (Waters et al. 2009), creating a diachronicity of the horizon. In the Swansea region, the base is contemporaneous with the Cambriense Marine Band at the base of the Llynfi Member (Barclay 2011) whilst the base rises as high in the stratigraphy as the Brithdir Member in the eastern coalfield (Waters et al. 2009). The top of the Pennant Sandstone is also diachronous with the Swansea Member absent in the east of the coalfield (Waters et al. 2009). The diachronous boundary means the variability of thickness of the Pennant is high (Figure 2), particularly across the Neath Disturbance, a major northeast–southwest trending Caledonoid fault in the modern Vale of Neath (Barclay 2011).

Correlation of the Pennant Sandstone between the Pembrokeshire and South Wales Coalfields is contentious with an early study suggesting correlation of Pembrokeshire outcrops with the Hughes Member (Jenkins 1962). More recently, a palaeobotanical study conducted by Cleal and Thomas (1992) correlated these deposits with the Rhondda Member. Herein, the Pembrokeshire Pennant is included in the Rhondda Member.

Although there has been little recent work on the sedimentology of the Pennant Formation, previous studies in the last 50 years have generally described the depositional environment of the Pennant Sandstone as a low-sinuosity, relatively proximal braidplain, characterised by development of sheet-like or stacked sandstone bodies, a concentration of in-channel bedforms and a general absence of point bar deposits (Kelling 1969; Jones 1977; Jones and Hartley 1993). The doctoral thesis of Jones (1977), for instance, includes extensive and detailed qualitative analyses of architectural features and facies within the lower Pennant, and identifies two major facies associations; the first is interpreted as the result of repeated incursions of small deltas, or crevasse deltas, into shallow bays, and the second, which is dominant after the Llynfi member, is interpreted to record braided rivers characterised by a variable discharge regime, which laterally migrated through a vegetated floodplain environment. Although Jones (1977) rejects the notion of the Pennant recording “classical” meandering channels (*sensu* Allen 1963) and estimates channel widths of order hundreds of metres, their thesis also suggests that individual channels may have had flow depths of >15 m based on channel body thicknesses, which would have been unusually deep for braided systems. This example serves to underscore the potential discrepancies between facies-derived reconstructions presented in the historic literature and morphodynamic considerations. Consequently, our work allows for a re-evaluation of the characteristics of this regionally significant Carboniferous fluvial system for the 21st Century.

Study Methods

Field Data Collection

Field data were collected in the South Wales Coalfield (17 localities) and Pembrokeshire Coalfield (2 localities) during two field campaigns in August and September 2021. All measurements were taken in channelized sandstone bodies and form the basis of the reconstruction and analysis of river morphologies in this study.

Cross-sets

Cross-sets in medium to very-coarse sands were measured to reconstruct the sizes of bedforms in Pennant rivers using the method of Leclair and Bridge (2001). This approach requires mean cross-set heights, so distributions of heights in individual cross-sets (n = 268) were measured to the nearest 10 mm at 10 cm intervals along the major axis of the cross-set (7 to 62 measurements per cross-set; Figure 3b). From these height distributions, mean cross-set heights, h_{xs}, were subsequently extracted. Maximum heights were also extracted from the distributions to derive a scaling factor between mean–maximum cross-set heights for each member of the Pennant Sandstone. This method has successfully been used previously on fluvial strata in Utah, USA (Lyster et al. 2021), and northwest Scotland (Ganti et al. 2019).

Cross-set height maxima were also measured at each locality (n = 1809; Figure 3d). Using the new mean–maximum height scaling factors, mean cross-heights were estimated for each measured maximum height, expanding the total dataset from 268 to 2077 mean cross-set heights.

Palaeocurrent directions were determined at each field site by measuring the dip and dip direction of cross-set lee slopes (n = 1038). Bedding measurements were also taken at each site or from geological maps (n = 58). Palaeocurrent measurements were subsequently unfolded using *Stereonet 11* (Allmendinger 2020) to correct for the dip of beds and therefore decipher true palaeocurrent directions of these palaeo-rivers.

Grain size

Where the height distribution of an individual cross-set was measured, the median grain size, D_{50}, was also estimated using the Wentworth grainsize classification (Wentworth 1922; Figure 3e) and converted to a numerical value in metres (e.g., 0.000375 m for medium sand, 0.0005 m for medium−coarse sand etc.). Grain-size photographs were also taken at each locality to later verify the estimated grainsize using *ImageJ* software (Rasband 2018). Grain-sizes exceeding sand grade were observed in some outcrops of the Pennant Sandstone, and typically occurred as isolated lenses at the base of channel fills (Figure 3f; c.f. Jones 1977; Jones & Hartley 1993). Distributions of these conglomeratic sediments were measured using the Wolman point count method (Wolman 1954) to extract D_{50} and were used to constrain the maximum possible, but rare, flow conditions in Pennant rivers.

Architectural fluvial elements

To validate the palaeohydrological reconstructions, the dimensions of larger scale architectural elements were independently measured (Figure 4). The heights of both channel fill sandstone packages and accretion packages (downstream and lateral) were quantified using a laser range finder (Haglöf Laser Geo) to a precision of 0.1 m (n = 116). These accretion packages, representing bar-scale clinoforms, provide a maximum bankfull flow depth where the total height of the bar-clinoform is visible, or where it can be extrapolated (Mohrig et al. 2000; Hajek and Heller 2012). These estimates of bankfull flow depth were used to validate flow depths calculated from cross-set heights. Where possible, accretion package widths were measured for channel width calculations (below) and outcrop-scale photographs were taken to show the fluvial architecture of each site (Figure 4).

Palaeohydrology

Flow depth

Cross-set heights represent a fraction of the original bedform height. Here, the scaling relation of Leclair and Bridge (2001) was used to convert mean cross-set height, h_{xs}, to mean bedform height, h_d:

$$h_d = 2.9(\pm 0.7)h_{xs} \qquad (1)$$

This relationship is based on the theoretical model of Paola and Borgman (1991) for bedform migration over random topography on the bed with negligible angle of climb. Here, uncertainty of the scaling factor (±0.7) represents the standard deviation of the dataset used by Leclair and Bridge (2001). To account for this uncertainty, a Monte Carlo uncertainty propagation method was used. 10^6 random values of the model parameter were generated between the uncertainty intervals (2.9 + 0.7 and 2.9 − 0.7 for Eq. 1) and were used to calculate h_d. This recovered 10^6 values of h_d which were subsequently carried forwards — Monte Carlo uncertainty propagation was used in all subsequent equations presented here with the stated uncertainties.

To estimate flow depth, H, the relationship of Bradley and Venditti (2017) was used:

$$H = 6.7h_d \qquad (2)$$

This relationship was derived following a revaluation of past work on dune−depth scaling relations that were deemed to be ineffective (Yalin 1964; van Rijn 1984; Julien and Klaassen 1995). The scaling factor in Eq. 2 (i.e., 6.7) at 50% uncertainty has a range of 4.4–10.1. A Monte Carlo propagation was again used between these values to accommodate this uncertainty. Any calculated values of H that exceeded 125% of the maximum measured package thickness at the field site were removed from the dataset at this stage (n = 89 out of more than 2000 cross-sets).

Palaeoslope

Slope, S, was reconstructed using estimates of D_{50} and H, and using the empirical method of Trampush et al. (2014), which is appropriate for the range of grain sizes used in this study. Here Slope, S, is given by:

$$\log S = \alpha_0 + \alpha_1 \log D_{50} + \alpha_2 \log H \qquad (3)$$

where α_0, α_1 and α_2 are constants given as −2.08 ± 0.036, 0.254 ± 0.016, and −1.09 ± 0.044 respectively. Monte Carlo uncertainty propagation was used to accommodate uncertainty in the constants (Trampush et al. 2014). Palaeoslope values were analysed both temporally (i.e., between members) and spatially (i.e., downstream).

Flow velocity and unit discharge

The equation of Manning et al. (1890) was used to derive flow velocity, U, and water discharge per unit width, Q_U, as $Q_U = U \times H$. Manning's equation is given as:

$$U = \frac{1}{n} H^{\frac{2}{3}} S^{\frac{1}{2}} \qquad (4)$$

where n, Manning's Roughness Coefficient, is approximated as 0.03 following Lyster et al. (2021). U is given in m s^{-1} and Q_U is given in m^2 s^{-1}. Q_U can be multiplied by an estimated width, W, to give total bankfull discharge, Q, in m^3 s^{-1}.

Fluvial style and channel widths

Determining the planform morphology of ancient river systems can be difficult as preservation of entire channels is rare in the rock record (Brierley 1989; Parker 1976; Lyster et al. 2022). Traditionally, facies analyses of architectural elements using vertical profiles and plan-view exposures of fluvial strata are used to classify ancient rivers as meandering, straight, anastomosing, or braided (Miall 1985). However, these analyses are most effective where outcrop is complete. Therefore, quantitative techniques using the Froude number (Fr), S, and aspect ratio (i.e., the ratio of channel width, W, to channel depth, H) of channels can also be implemented to determine fluvial style. Fr is calculated using:

$$Fr = \frac{U}{\sqrt{gH}} \qquad (5)$$

where g is gravitational acceleration.

Stability fields for braided and meandering channels can be reconstructed using plots of S/Fr against the inverse of channel aspect ratio (i.e., H/W as opposed to W/H), as the seminal work of Parker (1976) originally showed. Recently, Lyster et al. (2022) re-evaluated the stability fields of Parker (1976) using a new dataset of nearly 1700 modern rivers. They showed that H/W<0.02 characterises multi-thread systems and H/W>0.02 characterises single-thread systems, while S/Fr>0.003 characterises braided multi-thread systems and S/Fr<0.003 characterises anastomosing multi-thread systems. Here, these new insights were used to reconstruct channel planform for all members of the Pennant Formation.

The method of Greenberg et al. (2021) was used to quantify single-thread channel widths, W_C, where lateral accretion package widths, W_L, were observed at field sites (n = 23).

$$W_C = 2.34(\pm 0.13)W_L \qquad (6)$$

Where lateral accretion packages were partially preserved, W_L was estimated by extrapolating accretion surfaces using structural measurements of accretion surfaces relative to bedding. Monte Carlo uncertainty propagation was used with the bounds of the scalar in Eq. 6. To estimate channel belt width, W, outcrop widths were measured at each site as a constraint on maximum W. In addition, a channel aspect ratio described in the thesis of Jones (1977) of 1:56, based on field observations in the Pennant at Rhondda Fawr, was also used.

Results

Palaeohydrology

Distributions of height within individual cross-sets demonstrate a linear relationship between mean and maximum cross-set height (h_{xs} and h_{xsMax}), where h_{xs} is ~62% of the maximum cross-set height (Figure 5a). Separating these data by member resulted in similar scaling relations in the range $h_{xs} = 0.59h_{xsMax}$ to $h_{xs} = 0.65h_{xsMax}$ (Figure 5b). These scaling relationships are comparable to those reported by Lyster et al. (2021) for Upper Cretaceous fluvial strata in Utah, suggesting that mean cross-set heights scale predictably with cross-set maxima. Using these member-specific scaling relationships, n = 1809 cross-set height maxima were converted to mean cross-set heights, and these were used to supplement the n = 268 mean cross-set heights from measured distributions. Of these n = 2077 mean cross-set heights, the mean value is 0.12 m.

Mean cross-set heights correspond to median flow depths, H, in the Pennant Sandstone of 2.3 m using Eq. 1 and 2, while taking channel/accretion packages heights as a proxy for H gives a median of 2.45 m (Fig. 6a). This suggests that results are robust with only 4% of calculated flow depths exceeding 125% of the maximum measured package height at the corresponding locality (Supplement 3). Figure 6 further summarises the hydrodynamic properties (H, S, U, and Q_U) reconstructed for the Pennant

Formation and its constituent members. As each measured cross-set has been scaled, the median and interquartile ranges of reconstructed hydrodynamics, grouped by member, have been extracted and plotted as box plots. This grouping aims to maximise the potential to isolate any temporal trends in the data. Flow depths reconstructed for all members are typically ~2 m, with only the Llynfi having marginally more shallow channels than the succeeding members (Fig. 6a). Palaeoslopes show limited temporal variation with all members returning median slopes of 4–5 $\times 10^{-4}$ (y/x; 0.02–0.03°), values that are consistent with sand-bedded lowland rivers (Fig. 6b; Trampush et al., 2014). No statistically significant up-section change in S was observed. Values of U and Q_U similarly show limited temporal variation with median values ranging between 1.2–1.3 m s^{-1} and 2–3 m^2 s^{-1} respectively (Fig. 6c, d). Overall, results suggest that the hydrodynamics of fluvial systems in the Variscan foreland were remarkably similar throughout Pennant deposition. In the few outcrops in which conglomerates were observed, representing the coarsest fraction of the Pennant Formation, reconstructed flow velocities are greater (>1.9 m s^{-1}) and show greater variation (1.9–2.3 m s^{-1}) while Q_U is a factor of 1.5–2 greater than in the sand fraction (blue crosses, Fig. 6). These values likely reflect the flow dynamics of the largest discharge events that would have occurred in rivers of the upper Carboniferous South Wales foreland basin.

Palaeocurrent rose diagrams were produced for each locality using structural measurements of cross-set lee faces, unfolded to account for the dip of beds (Figure 7). A range of palaeocurrent directions were recovered with flow directions to the west more common (11/18 sites) than flow directions to the east. The variability in palaeocurrent between field sites of similar spatio-temporal setting in the Pennant may suggest that the sinuosity of the rivers was higher than previously reported. The overall dominant axial drainage of the Variscan Mountains matches the study of Jones (1977). It is important to stress, however, that outcrops belonging to each member would not necessarily formed part of a single fluvial system, as deposition in the Pennant clearly involved more than one river system in both temporal and spatial senses

Spatial variation of S between outcrops of the same member shows more marked trends, although the interquartile ranges of predictions overlap (Figure 8). The clearest of these trends can be seen in the Brithdir Member's three field sites, which show a westward decline in channel gradient from ~6 $\times 10^{-4}$ in the east to ~4 $\times 10^{-4}$ in the west. It is hypothesized here that our sites formed part of the same fluvial system, based on slope, palaeocurrent and the authors' observations of similar facies. The three westernmost localities in the Rhondda Member in the South Wales Coalfield also show decreasing S downstream although the facies evidence is less convincing that they comprise the same system here. The Llynfi and Hughes members do not have field sites showing evidence of being part of the same system and, given the spatial scale (>100 km), are interpreted as outcrops representing spatially separated but temporally equivalent river systems. It is noted that the Pembrokeshire Pennant, which is here correlated with the Rhondda Member, has palaeoslopes markedly greater than its apparent equivalents in the South Wales Coalfield, and the palaeogeographic relationship of these outcrops to the main part of the Pennant remains unclear, as previous authors have noted (e.g., Jones 1977; Jones and Hartley 1993).

Planform morphologies

Plausible estimates of the channel width of single threads in the Pennant Formation, W_C, and the channel belt width, W, are shown in Figure 9a. Mean W_C is 55 m and ranges from 12−106 m. In contrast, values of W using the channel body aspect ratio of Jones (1977) have a mean value of 137 m, while outcrop widths measured in this study have a mean value of ca. 210 m. Bankfull water discharges, Q_{bf}, calculated using W_C, have an interquartile range of 80–200 $m^3 s^{-1}$ and a median of 140 $m^3 s^{-1}$ (Figure 9b). Considering the entire channel belt, bankfull discharges using the outcrop width give an interquartile range of 440–760 $m^3 s^{-1}$ and a median of 560 $m^3 s^{-1}$ (Figure 9c), while using the ratio of Jones (1977) gives an interquartile range of 320–490 $m^3 s^{-1}$ and a median bankfull discharge of 400 $m^3 s^{-1}$ (Figure 9d).

A key question is whether Pennant rivers were single-thread or multi-thread. Figure 10 shows the inverse of channel aspect ratio (i.e., H/W as opposed to W/H) plotted against S/Fr for n = 1227 measured cross-sets with corresponding single-thread widths, and for n = 1569 cross-sets with corresponding outcrop widths. For all data points combined (n = 2820), only 0.3% of data points fall outside of the single-thread field of Parker (1976); however, this method has been recently recognised to disfavour multi-thread classification for geologic examples (c.f. Lyster et al. 2022).

Here, using the revised stability fields of Lyster et al. (2022), 94% of points calculated using the width scaling method of Greenberg et al. (2021) plot in the revised single-thread stability field of Lyster et al. (2022), which is expected as this method (Equation 6) recovers estimates of single-thread channel widths. Given that single thread widths appear to have been of order 50 m and that outcrop widths have mean values of ~200 m, but maximum values up to 300 m, it is reasonable to anticipate that multiple threads could have coexisted within channel belts. This is consistent with the observation that 90% of data points using our measured outcrop width, which give an upper limit on maximum channel active width, plot in the multi-thread stability field of Lyster et al. (2022). In detail, where multiple threads may have been present, it is likely that a few active threads existed rather than many active threads, given the comparative magnitudes of bar clinoform widths, thread widths and outcrop widths (e.g., Greenberg et al. 2021). Further, within the multi-thread stability field proposed by Lyster et al. (2022), it is noted that 97% of data points using measured outcrop width plot in the anastomosing field proposed by Lyster et al. (2022).

These results underline that reconstruction of channel planform depends on effective evaluation of channel width estimates alongside facies-based interpretations. Nevertheless, the results presented here suggest that both single-thread and anastomosing multi-thread planforms may have prevailed during Pennant deposition. Importantly, these results do not support the notion that the Pennant Formation preserves predominantly braided multi-thread systems (Kelling 1974; Jones and Hartley 1993).

Discussion

What did the rivers of the Pennant Sandstone look like?

The results of this study provide the first quantitative insights into ancient rivers of the Pennant Sandstone. This study finds that, although the rivers drained northwards from the Variscan Mountains in the South (Jones and Hartley 1993; Evans 2004), field results from most localities (11/18) suggest west-directed palaeoflow. Axial drainage is common in foreland basins and can be seen in the modern Ganges Basin, at the foot of the Himalayas, or the rivers of the upper Amazon Basin (Garcia-Castellanos 2002). Flow to the north would have been limited spatially by the presence of the Wales-Brabant High at the northern margin of the foreland basin (Opluštil and Cleal 2007).The landscape was relatively flat in the foreland with river gradients of 4–5 $\times 10^{-4}$ (0.02–0.03°), comparable to upper reaches of the continental Guadalquivir River, southern Spain, ($S = 3.9 \times 10^{-4}$; Baena-Escudero et al. 2016) and of the Ebro River, Northern Spain ($S = 6.7 \times 10^{-4}$; Ollero Ojeda 1990).

Rivers of the Pennant had individual threads with bankfull widths of ~50 m while channel belts spanned 100–300 m. Median flow depths were 2−3 m, implying median bankfull discharges of 390–560 $m^3\ s^{-1}$ across the channel belt. Channel morphodynamics and hydrodynamics remain similar up-section, within the propagated uncertainties, although channels were likely steeper in the Pennant of Pembrokeshire where conglomerates are more abundant and Variscan deformation is more pronounced. Channels with depths of 10 to 15 m were not reconstructed and no measured cross-sets that might suggest such large depths were observed.

The results presented here build on the spatially constrained study of Jones (1977) in which it is suggested that some rivers of the Rhondda Member could have been 5 times deeper and 3–8 times wider than those reconstructed in this study. While architectural elements large enough to reflect rivers of this size were not observed in this study, amalgamated sandstone packages were observed to reach large enough scales, so our results provide important constraints between insights that can be drawn from the bedform scale compared to the channel body scale. Jones and Hartley's (1993) study on the reservoir characteristics of the Pennant Sandstone presents a channel depth to width ratio of 1:5–15 based on channel fill deposits while we find a single-thread depth to width ratio of 1:15–30, greater by a factor of ~2, again based on depths derived from cross-set analysis.

Field evidence of in-channel woody clasts (Figure 11) and coal seams point to a heavily vegetated region, potentially with marked discharge variability (c.f. Jones, 1977), and prior analyses of palaeoflora suggest an ever-wet, tropical climate (Opluštil and Cleal 2007). Britain was palaeogeographically sub-equatorial (Scotese 2001) meaning tectono-climatic conditions may have been analogous to the modern Amazon and Congo basins. Given water discharges of 300–600 $m^3\ s^{-1}$ it is estimated that the ancient rivers had drainage areas of 4500–9500 km^2, based on an average precipitation rate of 2 $m\ yr^{-1}$ from modern equatorial rainforests (e.g., Amazon Rainforest; Sombroek 2001), and assuming water discharge scales with drainage area.

Various planforms likely existed over the course of these ancient rivers. Using outcrop widths as a proxy for channel belt widths, many of these rivers may have been multi-thread. Of these multi-thread rivers, quantitative analysis using estimates of slope and Froude number (Equations 3 and 5), and the stability fields of Lyster et al. (2022), suggest that multi-thread Pennant rivers were likely to have been anastomosing. There is, however, both facies-based and quantitative evidence for single-thread reaches in Pennant rivers. Facies evidence includes laterally dipping accretion surfaces representing meander growth while the correspondence between estimates of single-thread widths and outcrop widths for some localities of the Hughes and Llynfi Members also suggests some outcrops preserve rivers with a single-thread planform.

The anastomosing river planform morphologies implied by the results in this study suggest that Pennant rivers were likely more stable than previous interpretations of relatively proximal braided systems. Anastomosing rivers are often characterised by large, typically vegetated, mid-channel bars or islands, in contrast to the highly mobile barforms that are typically observed in braided systems (e.g., Makaske 2001). The abundant vegetation in the Variscan foreland in the Westphalian (Opluštil and Cleal 2007) would have acted as a stabilising agent for the river systems, generating the large, but spatially limited, sandstone bodies that occur between the extensive mudstone dominated landscapes in the valleys of South Wales.

Pennant rivers show limited temporal trends up-section in the South Wales Coalfield. This is interpreted to imply that sediment supply kept pace with subsidence rates in the Variscan foreland during the Bolsovian and Asturian, maintaining a similar fluvial topography in the depocentre (Burgess and Gayer 2000). Upstream to downstream trends, however, are more visible in the data, particularly for slope; in the Brithdir Member, slope decreases from ~6 $\times 10^{-4}$ to 4 $\times 10^{-4}$ across the >10 km plan view distance between three field sites.

The mean hydrodynamic parameters and morphologies of Pennant rivers are summarised in Figure 12. Figure 12 represents the morphology of a hypothetical modern fluvial system, using the parameters reconstructed in this study, which suggest anastomosing morphologies of ~200 m width and ~2.5 m flow depths were most common in the rivers of the Pennant.

Overall, this study is the first to apply quantitative palaeohydrological techniques to this regionally important system. Results suggest that Pennant rivers exhibited both anastomosing and single-threaded planforms with bankfull discharges up to 560 $m^3 s^{-1}$. To a first order, the rivers were similar in scale and tectonic setting to the modern Guadalquivir and Ebro rivers of Spain, and the upper Kuban River, Russia.

Future perspectives and challenges

The methods in this study show that it is now possible to quantify the hydrodynamics of ancient rivers in a way that is not possible for analyses restricted to qualitative approaches, even where the latter has the produced valuable insights (e.g., Kelling 1974; Jones 1977; Jones and Hartley 1993). This is particularly important where poor outcrop preservation limits architectural mapping. However, it is critically important to consider qualitative and facies-based evidence together to validate the quantitative reconstructions (e.g., Supplement 3). The combination of methodologies used in this study demonstrates how to tackle this issue in the rock record. Here, reconstructions of hydrodynamics using cross-set and grain size measurements (Leclair and Bridge 2001; Trampush et al. 2014; Bradley and Venditti 2017) are found to provide results in agreement with evidence and observations of, for instance, the heights of accretion packages. The reconstruction of anastomosing and single thread planforms is consistent with facies associations and bedforms previously documented in the Pennant Sandstone (Kelling 1969, 1974; Jones and Hartley 1993) but the data in this work also allow us to rule out some reconstructions such as channel depths as great as 15 m (c.f. Jones 1977), which are inconsistent with the scale of the dune-scale cross-set heights, and the implied original bedform heights, documented here. Recent theoretical work has continued to improve extraction of quantitative information from fluvial strata (e.g., Greenberg et al. 2021; Lyster et al. 2022) and further refinements will facilitate reconstructions in a broader number of ancient fluvial systems to greater resolution than previously possible.

As all the equations used in this study carry forward calculated parameters (e.g., slope calculations implement the previously calculated flow depths), errors and uncertainties are compounded in this type of analysis. This must be addressed carefully and, here, it is tackled using Monte Carlo uncertainty propagation. Despite this, the greatest confidence remains in parameters calculated early in the methodology, due to the potential for architectural validation (i.e., H) while uncertainty is greater in parameters calculated later in the workflow which require more assumptions to be made (i.e., Q_{bf}).

Moving beyond the scope of this study, further detailed work is required to identify and trace individual fluvial systems in the Pennant Sandstone, which will serve to better constrain upstream to downstream trends in these rivers and to constrain the pathways of sediment dispersal from the Variscan highlands in the south. Additionally, previous interpretations of wet climatic conditions throughout Pennant deposition, as well as the presence of conglomeratic channel fills and woody debris pointing to the occurrence of floods, could be used to better constrain potential palaeohydrological variability in these systems and the climate drivers behind this (Fielding et al. 2018; Leary and Ganti 2020). Assuming uncertainties are appropriately acknowledged, there is clear potential to apply the methodology used in this study to many more ancient fluvial systems on Earth, but also increasingly on other planetary surfaces including Mars, where high resolution imagery increasingly enables grain-sizes, bedforms, and larger scale architectures to be quantified (e.g., Edgar et al. 2018; Davis et al. 2019; Stack et al. 2019; Balme et al. 2020; Mangold et al. 2021).

Conclusion

During the Westphalian stage of the Upper Carboniferous, the Variscan foreland in South Wales was characterised by large fluvial systems that deposited over 1300 m of sediment over a period of approximately 4 Myr. The four-dimensional reconstruction of the ancient fluvial systems of the Pennant Formation presented in this study suggests these rivers had median flow depths of 2–3 m, median slopes of 4–5 $\times 10^{-4}$ (y/x), individual channel thread widths of a few tens of metres, and channel belt widths of 100–200 m — these ancient rivers likely possessed both anastomosing and single-thread reaches. These results correspond to median bankfull discharges of 390–560 $m^3\ s^{-1}$. The reconstructed depositional setting is consistent with modern rivers in similar tectonic regimes such as the Ebro and Guadalquivir rivers, Spain, and in climatically similar regions such as the upper Amazon Basin. Significantly, there is little variation in these key palaeohydrological and morphodynamic variables up-section through the five members of the Pennant.

This study provides new insights into river behaviour during the latter stages of supercontinent assembly. Despite rapid subsidence rates in the South Wales foreland basin, little temporal variation is observed in key hydrodynamics and morphodynamics up-section, which implies these ancient fluvial systems were relatively stable in a time of intense compressional tectonism. This first-of-its-kind study for Carboniferous rivers in the UK adds to the growing body of recent work applying quantitative techniques to fluvial strata (e.g., Ganti et al. 2019; Lyster et al. 2021) and builds on the significant, but aging, body of qualitative and facies-based fluvial sedimentological studies undertaken on the Pennant Sandstone. This work demonstrates the utility of reconstructing hydrodynamics and styles of ancient fluvial systems from quantitative field data and could be applied even where facies-based reconstructions are equivocal or where outcrop is limited.

Acknowledgements

The authors acknowledge research support from Imperial College London. We thank Gary Hampson and Cedric John for useful feedback on an early version of the manuscript.

Author contributions

JW: Data curation (lead), formal analysis (lead), investigation (lead), methodology (lead), visualization (lead), writing – original draft (lead), writing – review and editing (equal); **JM:** Data curation (supporting), investigation (supporting), writing – review and editing (supporting); **SL**: Data curation (supporting), formal analysis (supporting), investigation (supporting), methodology (supporting), supervision (equal), writing – review and editing (equal); **AW**: Data curation (supporting), formal analysis (supporting), investigation (supporting), methodology (supporting), supervision (equal), writing – review and editing (equal).

Data availability

All data generated or analysed during this study are included in this published article (and its supplementary information files).

References

Allen, J.R.L., 1963. The classification of cross-stratified units, with notes on their origin. Sedimentology, 2: 93–114.

Allmendinger, R. 2020. *Stereonet 11*. http://www.geo.cornell.edu/geology/faculty/RWA/programs/stereonet.html

Baena-Escudero, R., Guerrero-Amador, I., García-Martínez, B., & Carlos Posada-Simeón, J. 2016. Human activities and inundation risks in the plain of the Guadalquivir River (in the reach between palma del río and seville, spain). *Boletín de La Asociación de Geógrafos Españoles* , *72*, 572–534.

Balme, M. R., Gupta, S., Davis, J. M., Fawdon, P., Grindrod, P. M., Bridges, J. C., Sefton-Nash, E., & Williams, R. M. E. 2020. Aram Dorsum: An Extensive Mid-Noachian Age Fluvial Depositional System in Arabia Terra, Mars. *Journal of Geophysical Research: Planets*, *125*(5). https://doi.org/10.1029/2019JE006244.

Barclay, W.J. 2011. Geology of the Swansea district – a brief explanation of the geological map. *Sheet Explanation of the British Geological Survey.* 1:50,000 Sheet 247 Swansea (England and Wales).

Bhattacharya, J. P., & Tye, R. S. 2004. Searching for Modern Ferron Analogs and Application to Subsurface Interpretation. In *Regional to Wellbore Analog for Fluvial-Deltaic Reservoir Modeling: The Ferron Sandstone of Utah* (Vol. 50, pp. 39–57). American Association of Petroleum Geologists.

Bhattacharya, J. P., Copeland, P., Lawton, T. F., & Holbrook, J. 2016. Estimation of source area, river paleo-discharge, paleoslope, and sediment budgets of linked deep-time depositional systems and implications for hydrocarbon potential. *Earth-Science Reviews*, *153*, 77–110. https://doi.org/10.1016/j.earscirev.2015.10.013

Bradley, R. W., & Venditti, J. G. 2017. Reevaluating dune scaling relations. In *Earth-Science Reviews* (Vol. 165, pp. 356–376). Elsevier B.V. https://doi.org/10.1016/j.earscirev.2016.11.004

Bridge, J. S., & Mackey, S. D. 1992. A Theoretical Study of Fluvial Sandstone Body Dimensions. In *The Geological Modelling of Hydrocarbon Reservoirs and Outcrop Analogues* (pp. 213–236). John Wiley & Sons, Ltd. https://doi.org/https://doi.org/10.1002/9781444303957.ch14

Brierley, G. J. 1989. River planform facies models: the sedimentology of braided, wandering and meandering reaches of the Squamish River, British Columbia. *Sedimentary Geology*, *61*(1), 17–35. https://doi.org/10.1016/0037-0738(89)90039-0

Burgess, P. M., & Gayer, R. A. 2000. Late Carboniferous tectonic subsidence in South Wales: implications for Variscan basin evolution and tectonic history in SW Britain. In *Journal of the Geological Society* (Vol. 157).

Castelltort, S., Goren, L., Willett, S. D., Champagnac, J. D., Herman, F., & Braun, J. 2012. River drainage patterns in the New Zealand Alps primarily controlled by plate tectonic strain. *Nature Geoscience*, *5*(10), 744–748. https://doi.org/10.1038/ngeo1582

Chamberlin, E. P., & Hajek, E. A. 2019. Using bar preservation to constrain reworking in channel-dominated fluvial stratigraphy. *Geology*, *47*(6), 531–534. https://doi.org/10.1130/G46046.1

Cleal, C. J., & Thomas, B. A. 1992. Lower Westphalian D fossil plants from the Nolton-Newgale Coalfield, Dyfed (Great Britain). *Geobios*, *25*(3), 315–322. https://doi.org/10.1016/0016-6995(92)80002-U

Davis, J. M., Gupta, S., Balme, M., Grindrod, P. M., Fawdon, P., Dickeson, Z. I., & Williams, R. M. E. 2019. A Diverse Array of Fluvial Depositional Systems in Arabia Terra: Evidence for mid-Noachian to Early Hesperian Rivers on Mars. *Journal of Geophysical Research: Planets*, *124*(7), 1913–1934. https://doi.org/10.1029/2019JE005976

De la Beche, Sir H. 1846. On the formation of rocks of South Wales and South Western England. Memoirs of the Geological Survey. 1. 1-296.

Duller, R. A., Whittaker, A. C., Fedele, J. J., Whitchurch, A. L., Springett, J., Smithells, R., Fordyce, S., & Allen, P. A. 2010. From grain size to tectonics. *Journal of Geophysical Research: Earth Surface*, *115*(3). https://doi.org/10.1029/2009JF001495

Edgar, L. A., Gupta, S., Rubin, D. M., Lewis, K. W., Kocurek, G. A., Anderson, R. B., Bell, J. F., Dromart, G., Edgett, K. S., Grotzinger, J. P., Hardgrove, C., Kah, L. C., Leveille, R., Malin, M. C., Mangold, N., Milliken, R. E., Minitti, M., Palucis, M., Rice, M., … Williams, A. J. 2018. Shaler: in situ analysis of a fluvial sedimentary deposit on Mars. *Sedimentology*, *65*(1), 96–122. https://doi.org/10.1111/sed.12370

Eriksson, P. G., Bumby, A. J., Brümer, J. J., & van der Neut, M. 2006. Precambrian fluvial deposits: Enigmatic palaeohydrological data from the c. 2–1.9 Ga Waterberg Group, South Africa. *Sedimentary Geology*, *190*(1), 25–46. https://doi.org/10.1016/j.sedgeo.2006.05.003

Evans, B. G. 2004. An introduction to the South Wales Pennant Formation: its origin, outcrop and conservation. *Geologica Balcanica*, *34*.

Fielding, C. R., Alexander, J., & Allen, J. P. (2018). The role of discharge variability in the formation and preservation of alluvial sediment bodies. In *Sedimentary Geology* (Vol. 365, pp. 1–20). Elsevier B.V. https://doi.org/10.1016/j.sedgeo.2017.12.022

Ganti, V., Lamb, M. P., & McElroy, B. 2014. Quantitative bounds on morphodynamics and implications for reading the sedimentary record. *Nature Communications*, *5*. https://doi.org/10.1038/ncomms4298

Ganti, V., Whittaker, A. C., Lamb, M. P., & Fischer, W. W. 2019. Low-gradient, single-threaded rivers prior to greening of the continents. *Proceedings of the National Academy of Sciences of the United States of America*, *116*(24), 11652–11657. https://doi.org/10.1073/pnas.1901642116

Garcia-Castellanos, D. 2002. Interplay between lithospheric flexure and river transport in foreland basins. *Basin Research*, *14*(2), 89–104. https://doi.org/10.1046/j.1365-2117.2002.00174.x

Gayer, R., & Jones, J. 1989. The Variscan foreland in south Wales. *Proceedings of the Ussher Society*, *7*(2), 177–179.

Gayer, R., & Pesek, J. 1992. Cannibalisation of coal measures in the south wales coalfield-significance for foreland basin evolution. *Proceedings of the Ussher Society*, 8, 44-49

Gibling, M., & Davies, N. 2021. Palaeozoic landscapes shaped by plant evolution. Nature Geosci 5, 99–105. https://doi.org/10.1038/ngeo1376

Greenberg, E., Ganti, V., & Hajek, E. 2021. Quantifying bankfull flow width using preserved bar clinoforms from fluvial strata. *Geology*, *49*(9), 1038–1043. https://doi.org/10.1130/G48729.1

Hack, J. T. 1957. Studies of longitudinal stream profiles in Virginia and Maryland. *Shorter Contributions to General Geology 1956*.

Hajek, E. A., & Heller, P. L. 2012. Flow-depth scaling in alluvial architecture and nonmarine sequence stratigraphy: Example from the Castlegate Sandstone, Central Utah, U.S.A. *Journal of Sedimentary Research*, *82*(2), 121–130. https://doi.org/10.2110/jsr.2012.8

Harries, R. M. et al. 2021. Impact of climate on landscape form, sediment transfer and the sedimentary record. Earth Surface Processes and Landforms (2021) https://doi.org/10.1002/esp.5075.

Hartley, A. J., & Warr, L. N. 1990. Upper Carboniferous foreland basin evolution in SW Britain. *Proceedings of the Ussher Society*, *7*(3), 212–216.

Hjellbakk, A. 1997. Facies and fluvial architecture of a high-energy braided river: the Upper Proterozoic Seglodden Member, Varanger Peninsula, northern Norway. *Sedimentary Geology*, *114*(1), 131–161. https://doi.org/10.1016/S0037-0738(97)00075-4

Holbrook, J., & Wanas, H. 2014. A fulcrum approach to assessing source-to-sink mass balance using channel paleohydrologic paramaters derivable from common fluvial data sets with an example from the cretaceous of Egypt. *Journal of Sedimentary Research*, *84*(5), 349–372. https://doi.org/10.2110/jsr.2014.29

Ielpi, A., Rainbird, R. H., Ventra, D., & Ghinassi, M. 2017. Morphometric convergence between Proterozoic and post-vegetation rivers. Nature Communications, 8(1), 15250. https://doi.org/10.1038/ncomms15250

Jenkins, T. B. 1962. The Sequence and Correlation of the Coal Measures of Pembrokeshire. *Quarterly Journal of the Geological Society of London*.

Jones, C. M. 1977. The sedimentology of Carboniferous fluvial and deltaic sequences; the Roaches Grit Group of the south-west Pennines and the Pennant Sandstone of the Rhondda Valleys. *PhD Thesis*.

Jones, J. A. 1991. A mountain front model for the Variscan deformation of the South Wales coalfield. *Journal of the Geological Society*, *148*(5), 881 LP – 891. https://doi.org/10.1144/gsjgs.148.5.0881

Jones, J. A., & Hartley, A. J. 1993. Reservoir characteristics of a braid-plain depositional system: the Upper Carboniferous Pennant Sandstone of South Wales. *Geological Society, London, Special Publications*, *73*(1), 143 LP – 156. https://doi.org/10.1144/GSL.SP.1993.073.01.09

Julien, P. Y., & Klaassen, G. J. 1995. Sand-dune geometry of large rivers during floods. *Journal of Hydraulic Engineering*, *121*(9), 657–663. https://doi.org/10.1061/(ASCE)0733-9429(1995)121:9(657)

Kelling, G. 1969. The environmental significance of cross stratification parameters in an upper Carboniferous fluvial basin. *Journal of Sedimentary Research*, *39*(3), 857–875. https://doi.org/10.1306/74D71D52-2B21-11D7-8648000102C1865D

Kelling, G. 1974. Upper Carboniferous sedimentation in South Wales. In T. R. Owen (Ed.), *The Upper-Palaeozoic and Post-Palaeozoic rocks of Wales* (pp. 185–225). University of Wales Press.

Leary, K. C. P., & Ganti, V. 2020. Preserved Fluvial Cross Strata Record Bedform Disequilibrium Dynamics. *Geophysical Research Letters*, *47*(2). https://doi.org/10.1029/2019GL085910

Leclair, S. F., & Bridge, J. S. 2001. Quantitative Interpretation of Sedimentary Structures Formed by River Dunes. Journal of Sedimentary Research; 71 (5): 713–716. https://doi.org/10.1306/2DC40962-0E47-11D7-8643000102C1865D

Leopold, L. B., & Maddock Jr., T. 1953. The hydraulic geometry of stream channels and some physiographic implications. In *Professional Paper*. https://doi.org/10.3133/pp252

Leopold, L. B., & Wolman, M. G. 1960. River meanders. *Geological Society of America Bulletin*, *71*(6), 769–793. https://doi.org/10.1130/0016-7606(1960)71[769:RM]2.0.CO;2

Leveridge, B., & Hartley, A. J. 2006. The Variscan Orogeny : the development and deformation of Devonian/Carboniferous basins in SW England and South Wales. In P. J. Brenchley & P. F. Rawson (Eds.), *The Geology of England and Wales* (pp. 225–255). Geological Society of London.

Li, Y., Bhattacharya, J. P., Ahmed, S., & Garza, D. 2018. Re-evaluating the paleogeography of the river-dominated and wave-influenced Ferron notom delta, Southern central Utah: An integration of detailed facies-architecture and paleocurrent analysis. *Journal of Sedimentary Research*, *88*(2), 214–240. https://doi.org/10.2110/jsr.2018.9

Lyster, S. J., Whittaker, A. C., Allison, P. A., Lunt, D. J., & Farnsworth, A. 2020. Predicting sediment discharges and erosion rates in deep time—examples from the late Cretaceous North American continent. *Basin Research*, *32*(6), 1547–1573. https://doi.org/10.1111/bre.12442

Lyster, S. J., Whittaker, A. C., Hampson, G. J., Hajek, E. A., Allison, P. A., & Lathrop, B. A. 2021. Reconstructing the morphologies and hydrodynamics of ancient rivers from source to sink: Cretaceous Western Interior Basin, Utah, USA. *Sedimentology*, *n/a*(n/a). https://doi.org/10.1111/sed.12877

Lyster, S.J., Whittaker, A.C. and Hajek, E.A. 2022, Accepted. The problem of Paleo-planforms. Geology

Mahon, R.C. and McElroy, B. 2018. Indirect estimation of bedload flux from modern sand-bed rivers and ancient fluvial strata. *Geology*, 46(7), 579–582, https://doi.org/10.1130/G40161.1

Makaske, B. 2001. Anastomosing rivers: a review of their classification, origin and sedimentary products. *Earth-Science Reviews* (Vol. 53). https://doi.org/10.1016/S0012-8252(00)00038-6

Mangold, N., Gupta, S., Gasnault, O., Dromart, G., Tarnas, J. D., Sholes, S. F., Horgan, B., Quantin-Nataf, C., Brown, A. J., Mouélic, S. L., Yingst, R. A., Bell, J. F., Beyssac, O., Bosak, T., Calef, F., Ehlmann, B. L., Farley, K. A., Grotzinger, J. P., Hickman-Lewis, K., … Williford, K. H. 2021. Perseverance rover reveals an ancient delta-lake system and flood deposits at Jezero crater, Mars. *Science*, *374*(6568). https://doi.org/10.1126/science.abl4051

Manning, R., Griffith, J. P., Pigot, T. F., & Vernon-Harcourt, L. F. 1890. On the flow of water in open channels and pipes.

Miall, A. D. 1985. Architectural-element analysis: A new method of facies analysis applied to fluvial deposits. *Earth-Science Reviews*, *22*(4), 261–308. https://doi.org/10.1016/0012-8252(85)90001-7

Michael, N. A., Whittaker, A. C., Carter, A. & Allen, P. A. 2014. Volumetric budget and grain-size fractionation of a geological sediment routing system: Eocene Escanilla Formation, south-central Pyrenees. *GSA Bulletin* 126, 585–599. https://doi.org/10.1130/B30954.1

Mohrig, D., Heller, P. L., Paola, C., & Lyons, W. J. 2000. Interpreting avulsion process from ancient alluvial sequences: Guadalope-Matarranya system (northern Spain) and Wasatch Formation (western Colorado). *GSA Bulletin*, *112*(12), 1787–1803. https://doi.org/10.1130/0016-7606(2000)112<1787:IAPFAA>2.0.CO;2

Ollero Ojeda, A. 1990. Slope, sinuosity and channel patterns in the Ebro river. *Cuadernos de Investigación Geográfica*, *16*(0), 73. https://doi.org/10.18172/cig.985

Opluštil, S., & Cleal, C. J. 2007. A comparative analysis of some Late Carboniferous basins of Variscan Europe. *Geological Magazine*, *144*(3), 417–448. https://doi.org/10.1017/S0016756807003330

Paola, C., & Borgman, L. 1991. Reconstructing random topography from preserved stratification. *Sedimentology*, *38*(4), 553–565. https://doi.org/10.1111/j.1365-3091.1991.tb01008.x

Paola, C., & Mohrig, D. 1996. Palaeohydraulics revisited: palaeoslope estimation in coarse-grained braided rivers. *Basin Research*, *8*(3), 243–254. https://doi.org/10.1046/j.1365-2117.1996.00253.x

Parker, G. 1976. On the cause and characteristic scales of meandering and braiding in rivers. *Journal of Fluid Mechanics*, *76*(3), 457–480. https://doi.org/10.1017/S0022112076000748

Plink-Bjorklund, P. 2015. Morphodynamics of rivers strongly affected by monsoon precipitation: Review of depositional style and forcing factors. *Sedimentary Geology*, *323*. https://doi.org/10.1016/j.sedgeo.2015.04.004

Rasband, W. S. 2018. *ImageJ*. https://imagej.nih.gov/ij/

Rippon, J. H. 1996. Sand body orientation, palaeoslope analysis and basin-fill implications in the Westphalian A–C of Great Britain. *Journal of the Geological Society*, *153*(6), 881–900. https://doi.org/10.1144/gsjgs.153.6.0881

Sadler, P. M. 1981. Sediment Accumulation Rates and the Completeness of Stratigraphic Sections. *The Journal of Geology*, *89*(5), 569–584. https://doi.org/10.1086/628623

Scotese, C. R. 2001. Atlas of Earth History, Volume 1, Paleogeography. *PALAEOMAP Project*.

Sharma, S., Bhattacharya, J. P., & Richards, B. 2017. Source-to-sink sediment budget analysis of the Cretaceous Ferron Sandstone, Utah, U.S.A, using the fulcrum approach. *Journal of Sedimentary Research*, *87*(6), 594–608. https://doi.org/10.2110/jsr.2017.23

Shibata, K., Adhiperdana, B. G., & Ito, M. 2018. Quantitative reconstruction of cross-sectional dimensions and hydrological parameters of gravelly fluvial channels developed in a forearc basin setting under a temperate climatic condition, central Japan. *Sedimentary Geology*, *363*, 69–82. https://doi.org/10.1016/j.sedgeo.2017.10.014

Sombroek, W. 2001. Spatial and temporal patterns of Amazon rainfall: Consequences for the planning of agricultural occupation and the protection of primary forests. *Ambio*, *30*(7), 388–396. https://doi.org/10.1579/0044-7447-30.7.388

Stack, K. M., Grotzinger, J. P., Lamb, M. P., Gupta, S., Rubin, D. M., Kah, L. C., Edgar, L. A., Fey, D. M., Hurowitz, J. A., McBride, M., Rivera-Hernández, F., Sumner, D. Y., van Beek, J. K., Williams, R. M. E., & Aileen Yingst, R. 2019. Evidence for plunging river plume deposits in the Pahrump Hills member of the Murray formation, Gale crater, Mars. *Sedimentology*, *66*(5), 1768–1802. https://doi.org/10.1111/sed.12558

Strahan, A. 1899. The geology of the South Wales Coalfield. Part I. The country around Newport, Monmouthshire. 1st edit. *Memoirs of the Geological Survey*.

Straub, K. M., Duller, R. A., Foreman, B. Z., & Hajek, E. A. 2020. Buffered, Incomplete, and Shredded: The Challenges of Reading an Imperfect Stratigraphic Record. *Journal of Geophysical Research: Earth Surface*, *125*(3). https://doi.org/10.1029/2019JF005079

Trampush, S. M., Huzurbazar, S., & McElroy, B. 2014. Empirical assessment of theory for bankfull characteristics of alluvial channels. *Water Resources Research*, *50*(12), 9211–9220. https://doi.org/10.1002/2014WR015597

van Rijn, L. C. 1984. Sediment Transport, Part III: Bed forms and Alluvial Roughness. *Journal of Hydraulic Engineering*, *110*(12), 1733–1754. https://doi.org/10.1061/(ASCE)0733-9429(1984)110:12(1733)

Waters, C. N., Browne, M. A., Dean, M. T., & Powell, J. H. 2007. Lithostratigraphical framework for Carboniferous successions of Great Britain (Onshore). *British Geological Survey.*

Waters, C. N., Waters, R. A., Barclay, W. J., & Davies, J. R. 2009. A lithostratigraphical framework for the Carboniferous successions of southern Great Britain (onshore). *British Geological Survey.*

Wentworth, C. K. 1922. A Scale of Grade and Class Terms for Clastic Sediments. *The Journal of Geology*, *30*(5), 377–392.

Whittaker, A. C. 2012. How do landscapes record tectonics and climate? *Lithosphere*, *4*(2), 160–164. https://doi.org/10.1130/RF.L003.1

Williams, G. P. 1984. Paleohydrological Methods and Some Examples from Swedish Fluvial Environments II—River Meanders. *Geografiska Annaler: Series A, Physical Geography*, *66*(1–2), 89–102. https://doi.org/10.1080/04353676.1984.11880101

Wolman, G. M. 1954. A method of sampling coarse river-bed material. *American Geophysical Union* (Vol. 35, Issue 6).

Woodland, A. W., Evans, W. B., & Stephens, J. v. 1957. Classification of the Coal Measures of South Wales with special reference to the Upper Coal Measures. *Bulletin of the Geological Survey of Great Britain. No. 13.* (pp. 6–13).

Xu, J., Snedden, J. W., Galloway, W. E., Milliken, K. T., & Blum, M. D. 2017. Channel-belt scaling relationship and application to early Miocene source-to-sink systems in the Gulf of Mexico basin. *Geosphere*, *13*(1), 179–200. https://doi.org/10.1130/GES01376.1

Yalin, M. S. 1964. Geometrical Properties of Sand Waves. *Journal of Hydraulic Engineering*, *90*, 105–119.

Figure Captions

Fig. 1 – (**a**) Location map showing the extent of the Pennant Sandstone Formation in South Wales, UK. (**b**) Geological map of the primary study area, the South Wales Coalfield with field sites shown (excludes Pembrokeshire localities). Contains British Geological Survey materials ©UKRI 2021. (**c**) Simplified paleogeographic reconstruction of England and Wales in the Westphalian Stage. Modified after Burgess and Gayer (2001) and Opluštil and Cleal (2007).

Fig. 2 - Stratigraphy of the Pennant Sandstone Formation, correlated across the Neath Disturbance (major N-S trending Caledonoid fault). Major named coal seams are indicated. Approximate stratigraphic interval of this study's field sites also shown. Modified after (Barclay 2011) with age data from BGS Geological Timechart.

Fig. 3 - Selected field photographs. (**a-d**) Cross-sets of the Pennant Sandstone (a-b = Rhondda Member, c-d = Brithdir Member). (**b & d**) Interpreted cross-sets in photos (**a & c**). Cyan lines show where height measurements were taken for distributions, red lines show where cross-set height

maxima were measured. (**e**) Grain size photograph of medium sand fraction, D50 = 0.375 mm. (**f**) Grain size photograph of conglomeratic lag in the Pennant Sandstone Formation, D50 = 9 mm.

Fig. 4 - Selected photographs and architectural interpretations of field localities of each member of the Pennant Sandstone. Note channel and accretion packages are not distinguished here but package type was noted at each example. (**a & b**) Swansea Member; (**c & d**) Hughes Member; (**e & f**) Brithdir Member; (**g & h**) Rhondda Member; (**I & j**) Llynfi Member.

Fig. 5 - Plots of measured mean cross-set height from distributions (n = 268) against maximum cross set heights, separated into (**a**) plot of data from all Pennant Sandstone Formation and (**b**) plot of data separated by member within the formation. Scaling relationships are derived from a linear regression through the origin of the dataset.

Fig. 6 - Boxplots of palaeohydrological characteristics of the rivers of the Pennant Sandstone Formation and each of its members. Every cross-set measured in each member is represented in the median and interquartile range of each plot. Conglomerate fraction indicated by blue cross (no conglomerate present in Brithdir Member). Median package height for each member is indicated as green cross on flow depth plots.

Fig. 7 - Palaeocurrent rose diagrams using field data from each field site in the (**a**) South Wales Coalfield and (**b**) Pembrokeshire Coalfield. Although there is variability with some northwards directed currents, flow is predominantly to the west in the Pennant Sandstone Formation (11/18 localities). It is also unclear if our localities of the same member represent the same fluvial system.

Fig. 8 - Trampush et al. (2014) palaeoslope boxplots for each locality arranged by longitude showing possible downstream trend in palaeoslope. Pemb. = Pembrokeshire Coalfield. Legend as Fig. 6. Note. field sites in each member are not known to be of the same fluvial system. Swansea member is not included here as field sites do not show sufficient spatial variation.

Fig. 9 - Summary of single-thread and channel belt widths and discharges in the Pennant Sandstone Formation. (**a**) Widths calculated using the methods of Jones (1977; error = interquartile range), Greenberg et al. (2021; error = standard error of Eq. 6), and the outcrop width. Arranged by locality, west-east. (**b-d**) Cumulative frequency plots of water discharge assuming widths shown here and unit discharges (Figure 6d) for each member. (**b**) Single-thread discharges using Greenberg et al. (2021). (**c**) Channel belt discharge using outcrop width. (**d**) Channel belt discharge using Jones (1977) width.

Fig. 10 - Plot predicting the fluvial style of the Pennant Sandstone Formation. Plot of H/W against S/Fr using width estimates from Greenberg et al. (2021) and the outcrop width. Stability fields for

single- and multi-threaded systems of Parker (1976; grey dashed line) and Lyster et al. (2022; red/green dashed lines) are shown.

Fig. 11 - Photograph of large wood clast in the Hughes Member.

Fig. 12 - Graphical representation of the ancient rivers of the Pennant Sandstone. (**a**) Mean single-thread channel cross section. (**b**) Average planform morphology. Note: single-threaded river sections also exist but are not represented here. (**c**) Longitudinal cross-section showing mean flow depths, dune heights and palaeoslopes. Note: slope is heavily exaggerated.

figure 1

Click here to access/download;figure;Figure 1 - Location Map.pdf

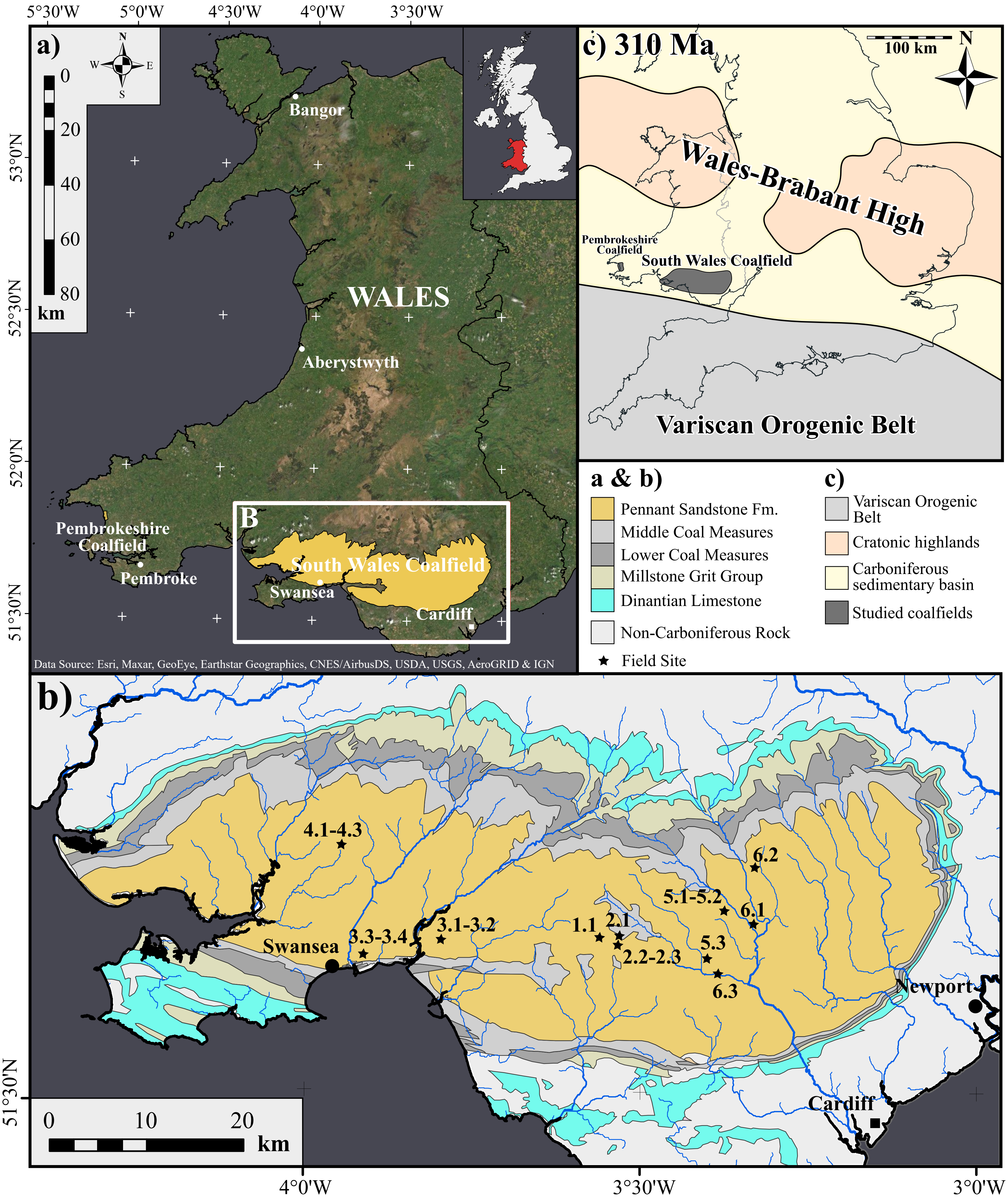

figure 2

Click here to access/download;figure;Figure 2 - Stratigraphic Column.pdf

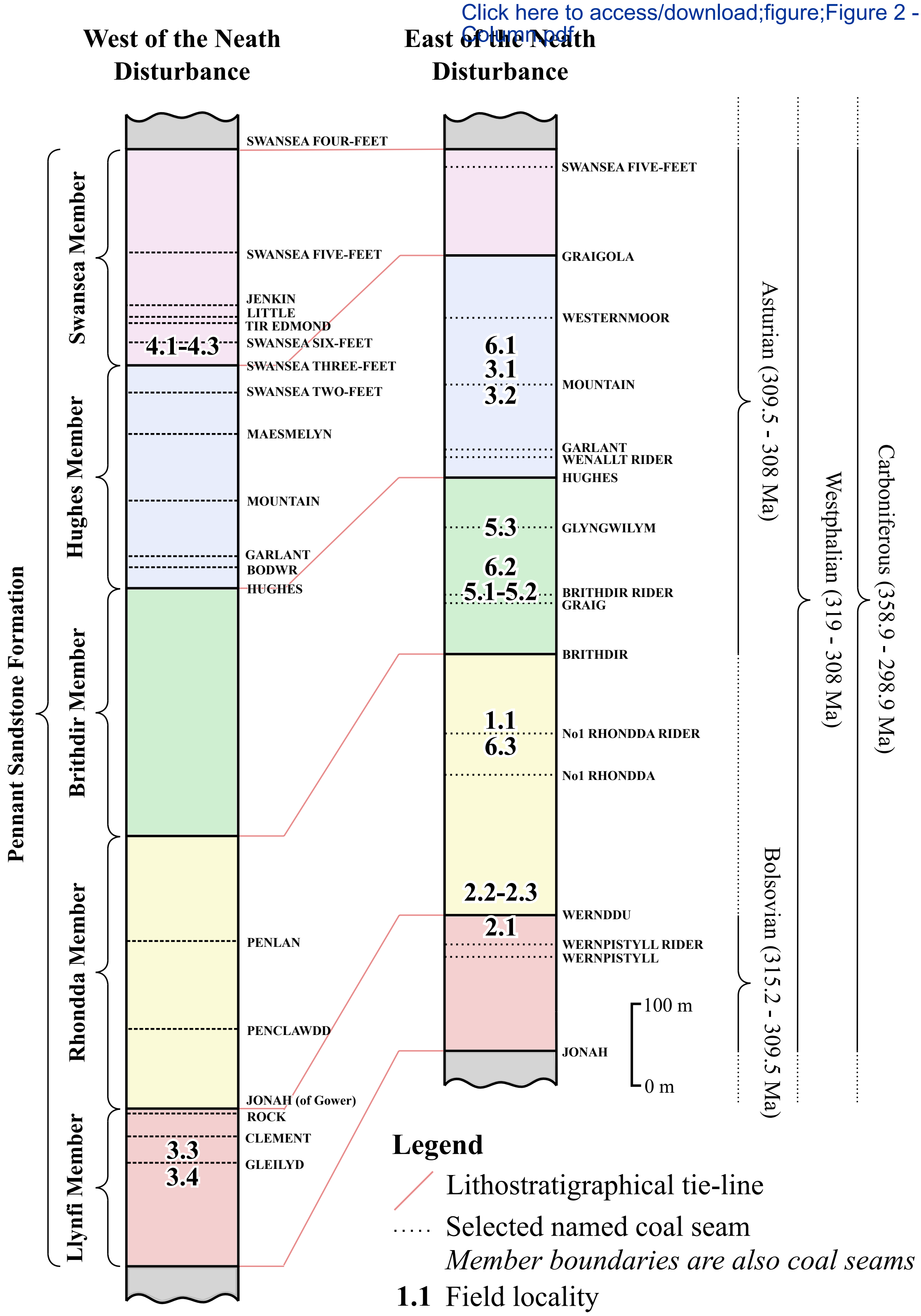

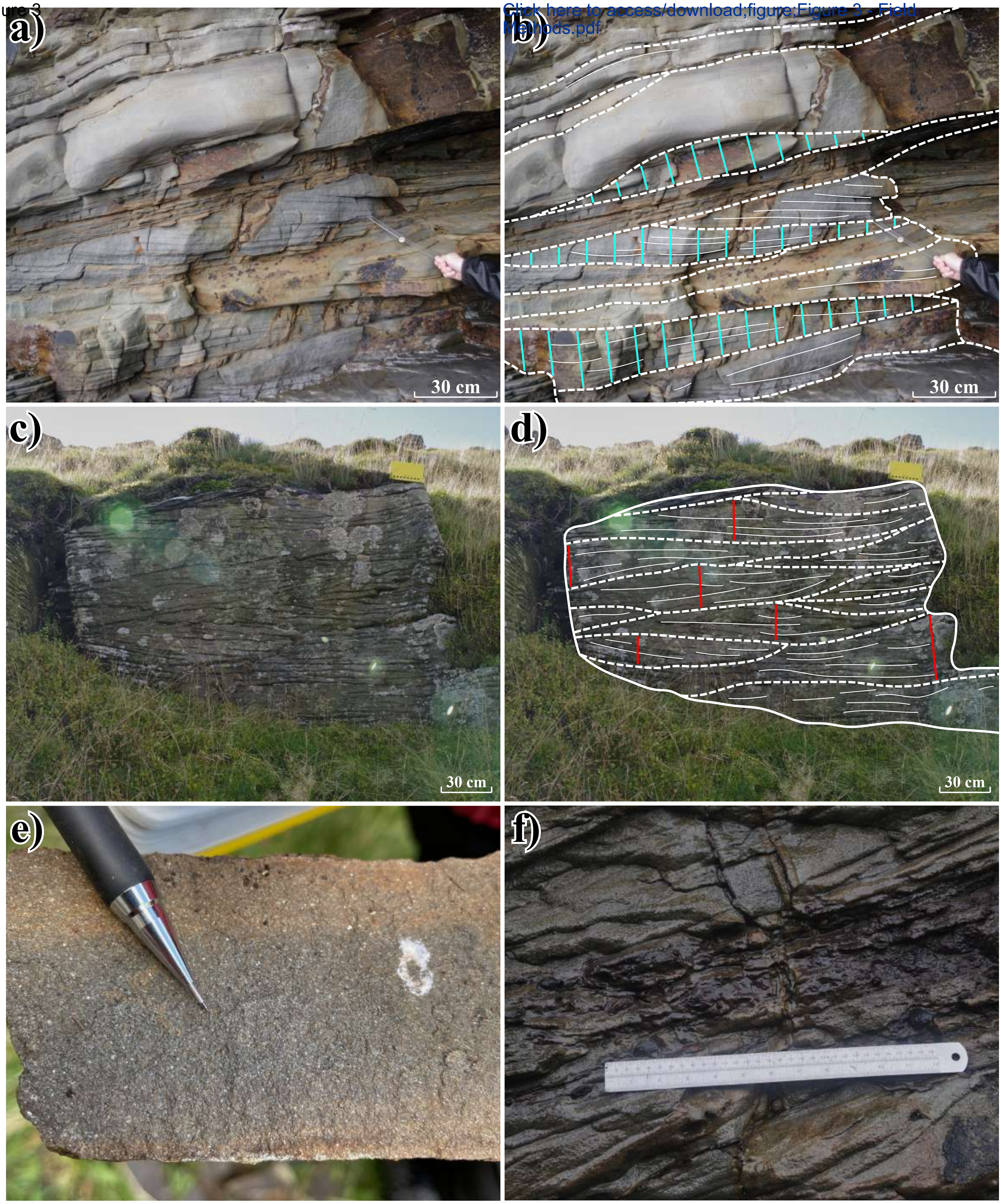
a)
30 cm
b)
30 cm
c)
30 cm
d)
30 cm
e)
f)

figure 4


a)
b)
c)
d)
e)
f)
g)
h)
i)
j)
10 m
10 m
2 m
5 m
10 m
Accretion/channel packages
Accretion/bedding surfaces
Vegetation

figure 5

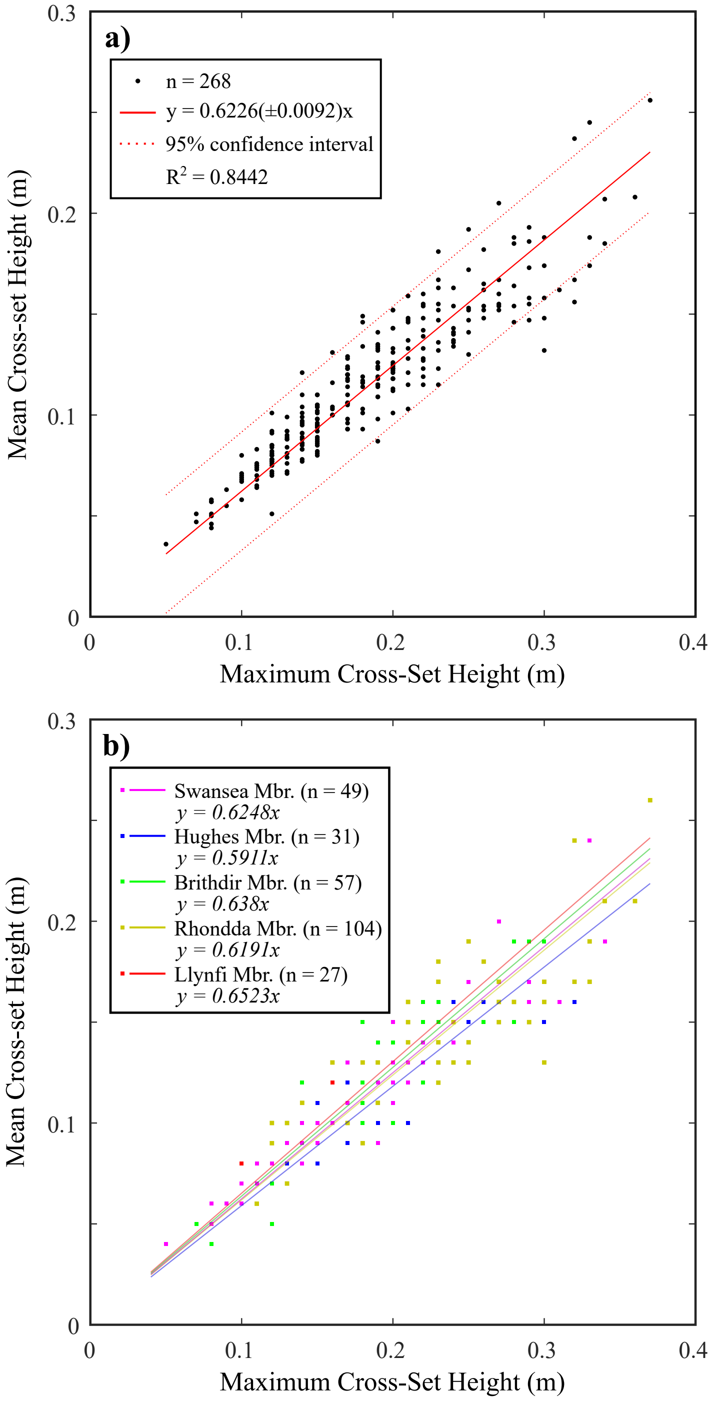
a)
n = 268
y = 0.6226(±0.0092)x
95% confidence interval
R² = 0.8442
Mean Cross-set Height (m)
Maximum Cross-Set Height (m)
0
0.1
0.2
0.3
0.4
b)
Swansea Mbr. (n = 49)
y = 0.6248x
Hughes Mbr. (n = 31)
y = 0.5911x
Brithdir Mbr. (n = 57)
y = 0.638x
Rhondda Mbr. (n = 104)
y = 0.6191x
Llynfi Mbr. (n = 27)
y = 0.6523x
Mean Cross-set Height (m)
Maximum Cross-Set Height (m)

figure 6

Click here to access/download;figure;Figure 6 - Palaeohydrology.pdf

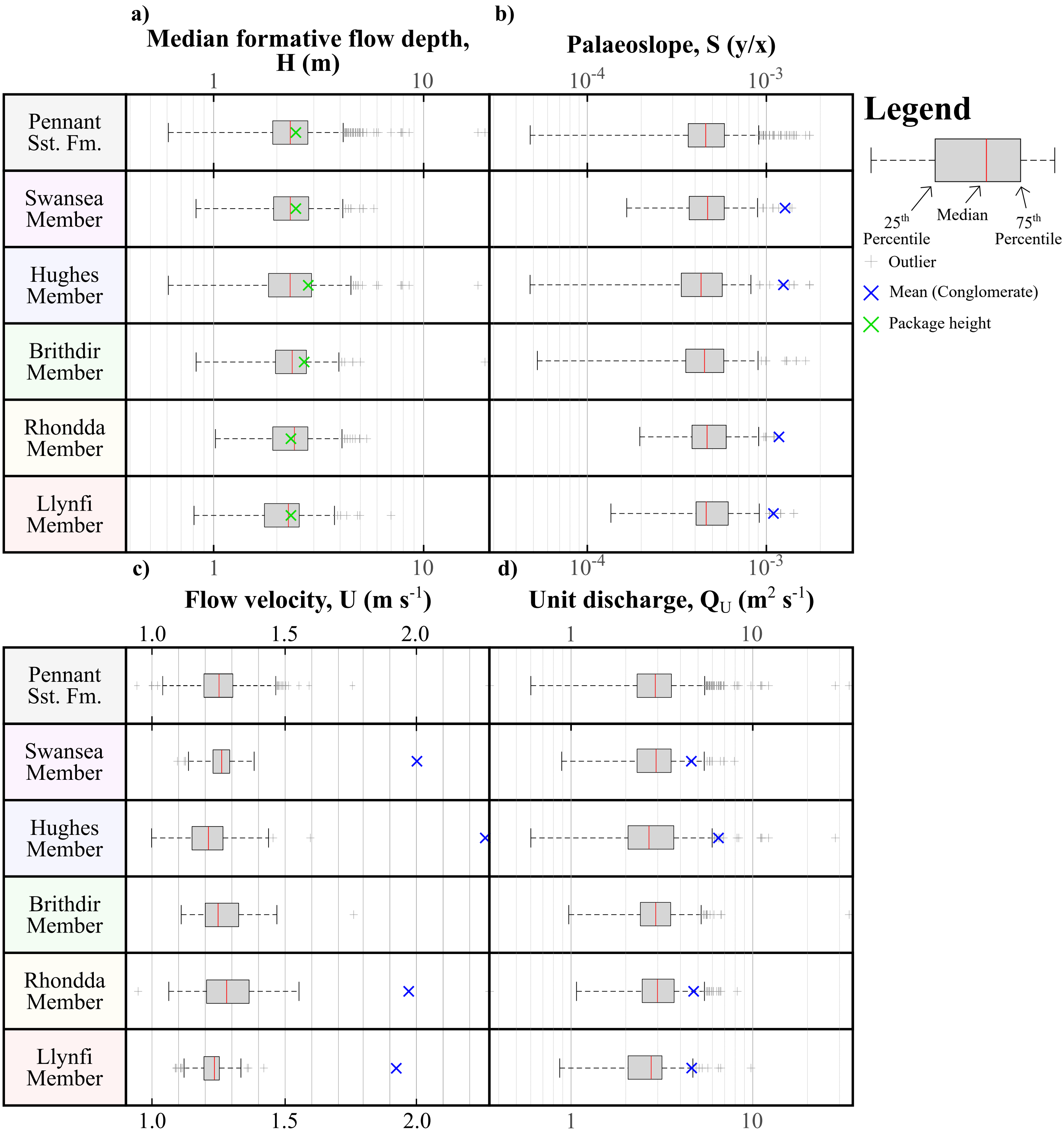

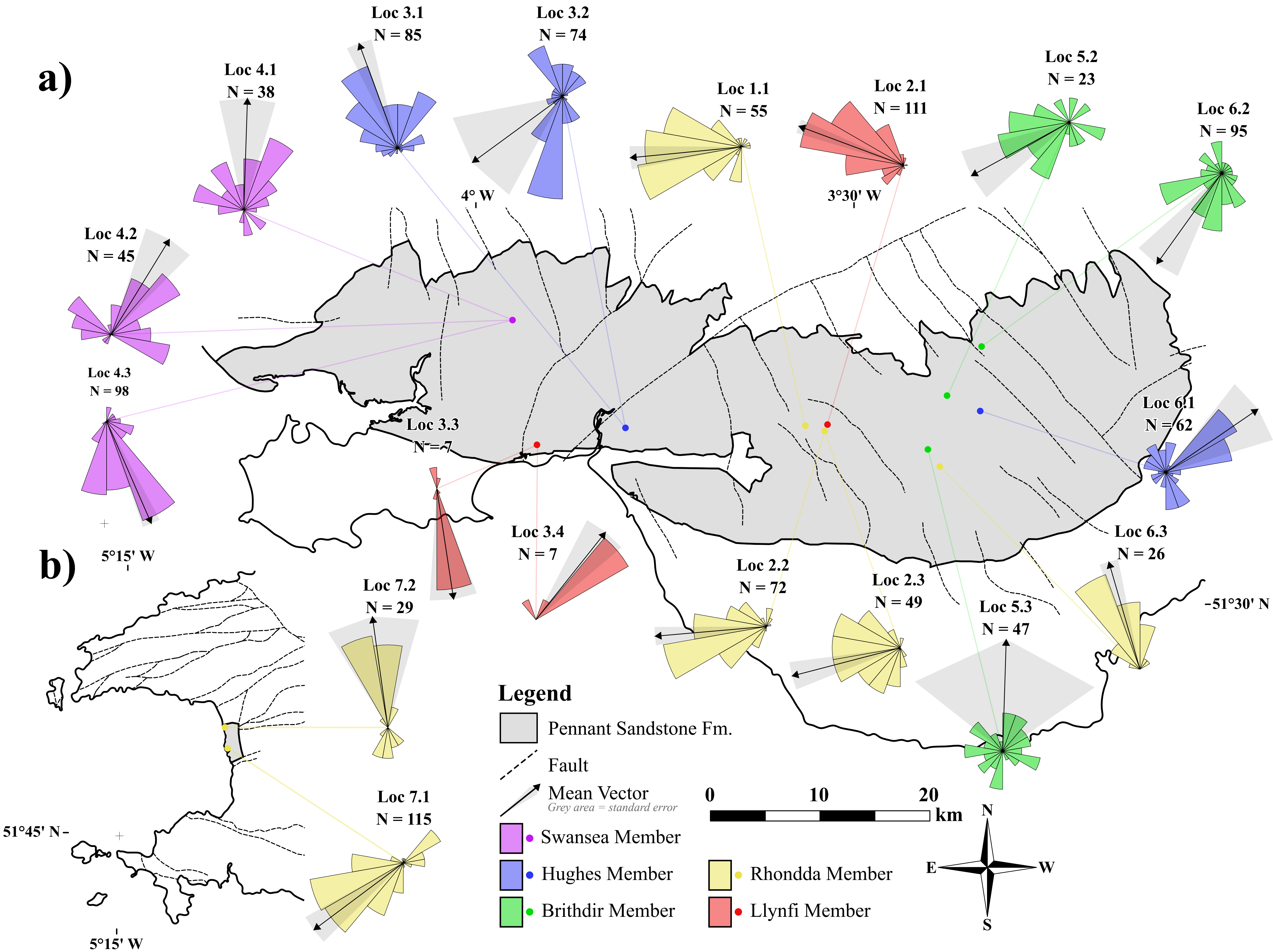
a)
b)
Loc 3.1
N = 85
Loc 3.2
N = 74
Loc 4.1
N = 38
Loc 1.1
N = 55
Loc 2.1
N = 111
Loc 5.2
N = 23
Loc 6.2
N = 95
Loc 4.2
N = 45
Loc 4.3
N = 98
Loc 3.3
N = 7
Loc 3.4
N = 7
Loc 6.1
N = 62
Loc 6.3
N = 26
Loc 2.2
N = 72
Loc 2.3
N = 49
Loc 5.3
N = 47
Loc 7.2
N = 29
Loc 7.1
N = 115
4° W
3°30' W
5°15' W
51°30' N
51°45' N
5°15' W
Legend
Pennant Sandstone Fm.
Fault
Mean Vector
Grey area = standard error
Swansea Member
Hughes Member
Brithdir Member
Rhondda Member
Llynfi Member
0
10
20
km
N
E
W
S

figure 8

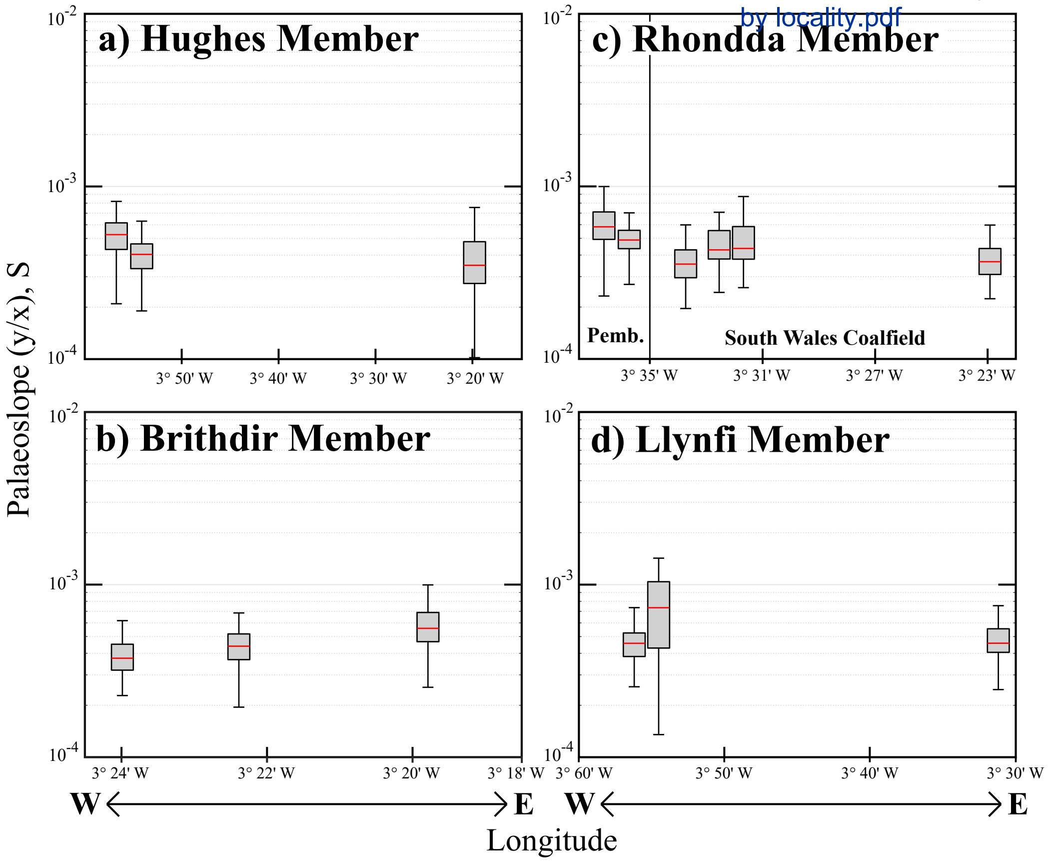
a) Hughes Member
b) Brithdir Member
c) Rhondda Member
d) Llynfi Member
Pemb.
South Wales Coalfield
Palaeoslope (y/x), S
3° 50' W
3° 40' W
3° 30' W
3° 20' W
3° 35' W
3° 31' W
3° 27' W
3° 23' W
3° 24' W
3° 22' W
3° 20' W
3° 18' W
3° 60' W
3° 50' W
3° 40' W
3° 30' W
W
E
W
E
Longitude

figure 9

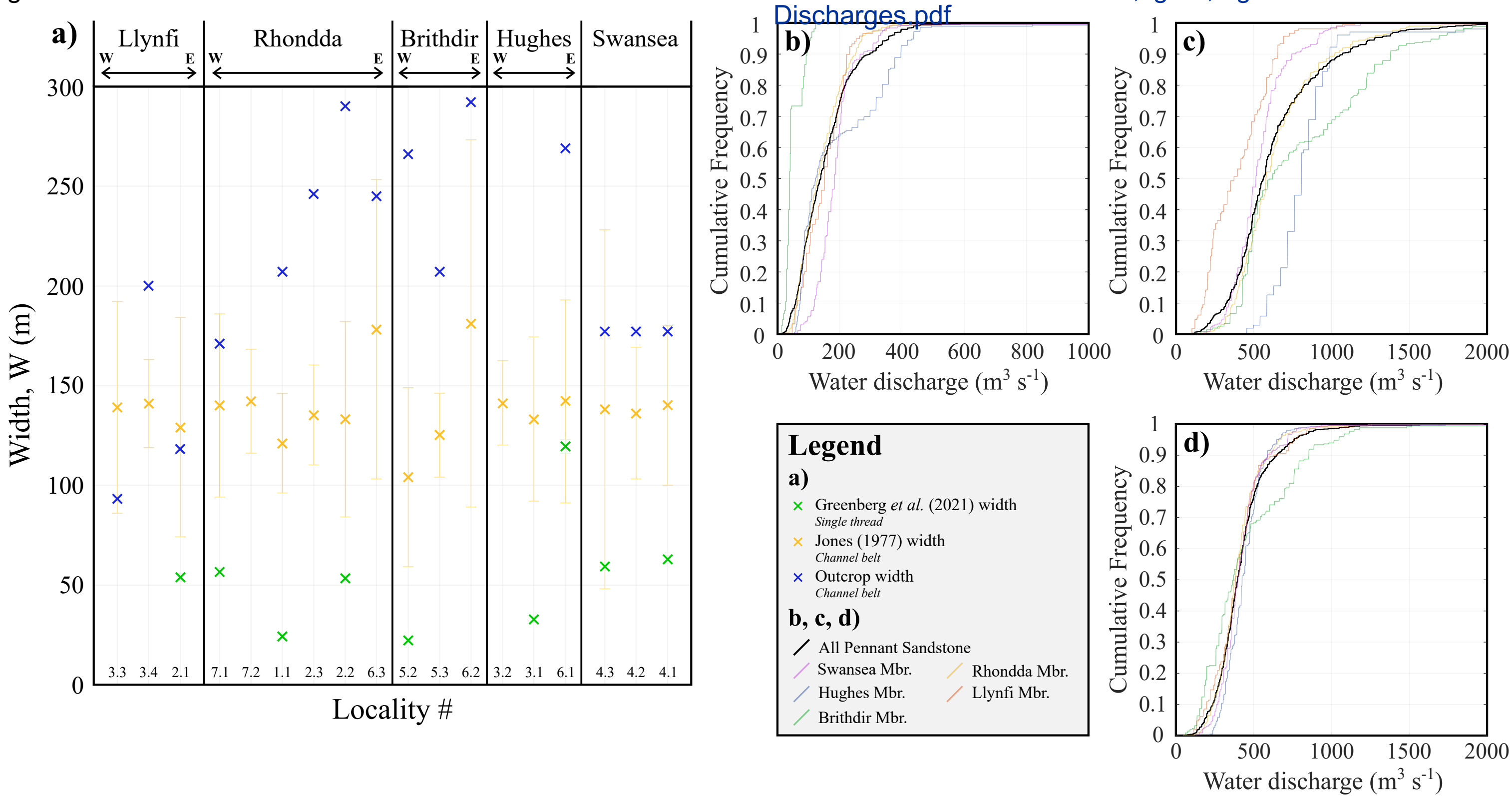
a)
Llynfi
Rhondda
Brithdir
Hughes
Swansea
W
E
Width, W (m)
Locality #
3.3 3.4 2.1 7.1 7.2 1.1 2.3 2.2 6.3 5.2 5.3 6.2 3.2 3.1 6.1 4.3 4.2 4.1
b)
c)
d)
Cumulative Frequency
Water discharge (m^3 s^{-1})
Legend
a)
Greenberg *et al.* (2021) width
Single thread
Jones (1977) width
Channel belt
Outcrop width
Channel belt
b, c, d)
All Pennant Sandstone
Swansea Mbr.
Rhondda Mbr.
Hughes Mbr.
Llynfi Mbr.
Brithdir Mbr.

figure 10

Click here to access/download;figure;Figure 10 - Fluvial Style.pdf

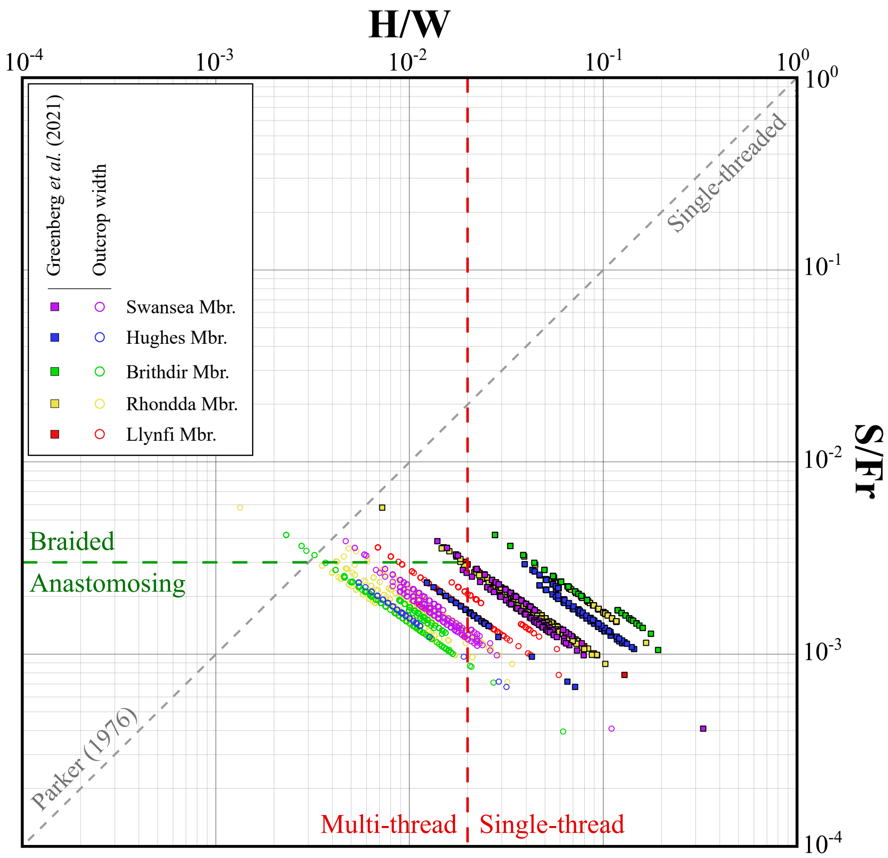

figure 11

Click here to access/download;fig

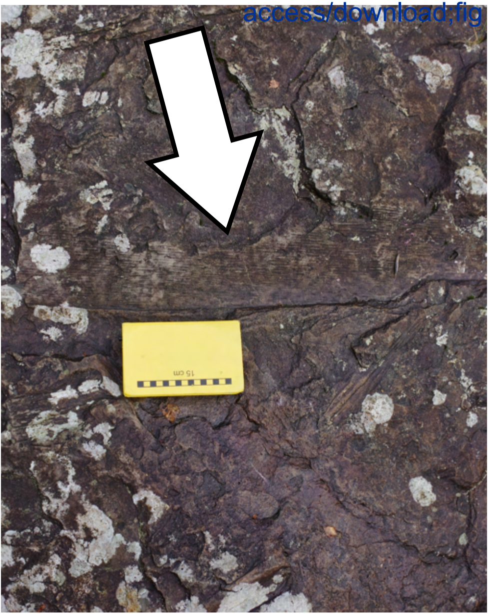

figure 12

Click here to access/download;figure;Figure 12 - Morphodynamic Summary.pdf

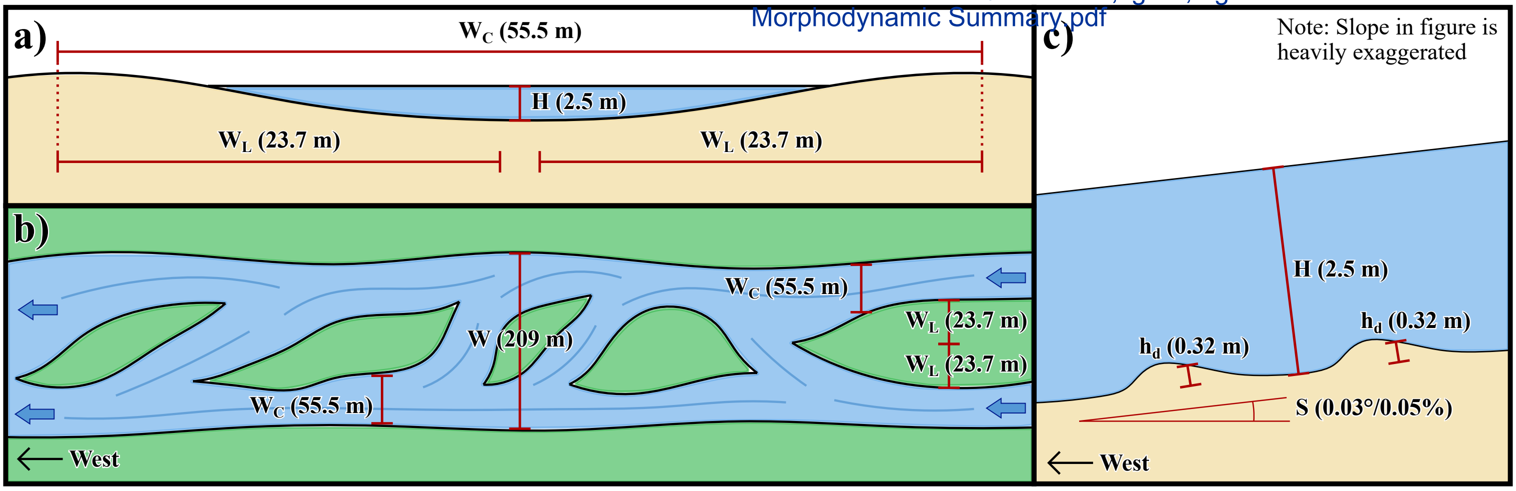

supplementary material text

Click here to access/download
supplementary material
Rivers of the Variscan Foreland - Supplementary Information.docx

Click here to access/download
supplementary material
Field Data.xlsx

supplementary material - field localities KMZ

Click here to access/download
supplementary material
doc.kml

supplementary figure - S1 - Scaling verification

Click here to access/download
supplementary material
Figure S1 - Scaling Verification.pdf

supplementary figure - S2 - facies rose diagrams

Click here to access/download
supplementary material
Figure S2 - Facies Rose Diagrams.pdf